# Braided deltas and diagenetic control on tight sandstone reservoirs: A case study on the Permian Lower Shihezi Formation in the southern Ordos Basin (central China)

Yang Li [a], Aiping Fan [a,*], Renchao Yang [a,b], Yipu Sun [c], Nils Lenhardt [d]

[a]Shandong Provincial Key Laboratory of Depositional Mineralization & Sedimentary Minerals, Shandong University of Science and Technology, Qingdao 266590, China

[b]Laboratory for Marine Mineral Resources, Qingdao National Laboratory for Marine Science and Technology, Qingdao 266071, China

[c]Sinopec Petroleum Exploration and Production Research Institute, Beijing 100083, China

[d]Department of Geology, University of Pretoria, Private Bag X20, 0028 Pretoria, South Africa

*Corresponding author. Email: xiaofansdust@163.com

## Highlights

- Braided delta facies dominate the Lower Shihezi Formation in the south of Ordos.
- Reservoir properties are controlled by sedimentary microfacies and diagenesis.
- Compaction, cementation and dissolution developed in the sandstone reservoir.
- Differences in sedimentary facies are the dominant factor controlling sandstone reservoir quality.

## Abstract

The Lower Shihezi Formation, situated in the south of the Chinese Ordos Basin, is a tight sandstone reservoir that is generally influenced by its sedimentary facies and diagenesis, corresponding to distinct petrophysical reservoir properties for each lithofacies type. The existing lithofacies types within the Lower Shihezi Formation were determined through observations in field profiles and drill cores that were combined with the analysis of logging data. Diagenetic processes and their effects were analyzed by using different methods, such as conventional thin section, cast thin section, and scanning electron microscope (SEM) analyses. The results of this contribution indicate that the Lower Shihezi Formation in the southern Ordos Basin is dominated by braided delta facies and locally developed lacustrine facies. During diagenesis of this studied formation, compaction and cementation led to a reduction in porosity with compaction probably forming the main factor. Existing cementation is mainly manifested in the form of clay mineral cements, siliceous and carbonate cements, and induced a somewhat lower pore reduction effect on the reservoir compared to compaction. Minor dissolution led to the break-down of rock fragments, feldspars, and other soluble minerals, and thereby may have caused a subsequent formation of secondary pores, thus effectively improving the reservoir property. Consequently, due to the compositional differences and corresponding unique diagenetic effects, the distributary channels and underwater distributary channels display the highest reservoir properties. These are followed by the mouth bars and sand sheets. The lowest reservoir properties are shown by the natural levee microfacies.

**Keywords:** Ordos Basin; Lower Shihezi Formation; Tight sandstone reservoirs; Sedimentary facies; Diagenesis; Reservoir quality

## 1. Introduction

Tight sandstone reservoirs are unconventional (hydrocarbon) reservoir rocks with low porosities and permeabilities (porosities of less than 10%, permeabilities less than 0.1 mD), and exhibit large heterogeneities in their reservoir properties (Zhao et al., 2012). Nevertheless, despite much lower porosities and permeabilities compared to those of conventional reservoirs, tight sandstone reservoirs exhibit a high exploration and development potential as they can develop into high-quality reservoirs (Liu et al., 2013; Zou et al., 2018; Sun et al., 2019; Qin et al., 2021). With the growth of the global demand for oil/natural gas and the reduction of conventional oil/natural gas production, tight sandstone oil and gas, as an important alternative resource, has increasingly attracted the attention of international scholars (e.g., Hu et al., 2018). After initial successful tight sandstone oil and gas development in countries such as Canada, Australia, and Ecuador (Gaibor et al., 2008; Ghanizadeh et al., 2015), today, the exploration and development of tight sandstone oil and gas are carried out in many countries and regions throughout the world (Zou et al., 2012; S. Li et al., 2021). So far, the areas where tight sandstone gas reservoirs may be most concentrated are the Rocky Mountain, Akoma, Appalachia, Denver, San Juan, and Green River basins in North America (Masters, 1979; Curtis et al., 2012).

It is commonly accepted that the principal factors dominating the physical reservoir properties of tight sandstones are the grain sizes of their clastic particles, their composition, and diagenesis (Li et al., 2008; Huang et al., 2009). Accordingly, under equal compaction conditions, the pores and throats of coarse-grained reservoirs are usually larger than those of finer-grained reservoirs (Yu et al., 2020). Different compositions of sedimentary grains may respond differently during diagenesis and thereby may affect the reservoir (Morad et al., 2010). The grain sizes and grain composition, in turn, are mainly dominated by the provenance and sedimentary facies (Garzanti, 2019; Y. Li et al., 2021). Furthermore, during diagenesis, the selective combination of a multitude of possible diagenetic processes may also result in significantly different reservoir characteristics (Yang et al., 2020). For instance, compaction and cementation can reduce the porosity of the reservoir, but dissolution can ameliorate the physical properties.

In recent years, tight sandstone gas has been found in many sedimentary basins throughout China. Among these, the southern Ordos Basin exhibits abundant upper Paleozoic tight sandstone gas reservoirs that are characterized by strong heterogeneities (Yang et al., 2012; Xiao et al., 2019; S. Li et al., 2021). Successful exploration of sandstone reservoirs generally hinges on the precise research on the sedimentation and the understanding of the relevance between the depositional setting, diagenesis, and the resulting reservoir quality (Bjørlykke, 2014). Existing studies show that the reservoir quality of the Shanxi Formation in the south of the Ordos Basin is controlled by sedimentary and diagenetic characteristics (Yang et al., 2012; Xiao et al., 2019; S. Li et al., 2021). There are great differences in sedimentary facies and diagenesis between the Lower Shihezi Formation and the Shanxi Formation (Yang et al., 2012; Y. Li et al., 2021), and there is a lack of systematic research on the Lower Shihezi Formation. Consequently, this contribution aims to provide detailed new information on the reservoir, sedimentation, and diagenesis of the Upper Paleozoic Lower Shihezi Formation. In addition, we will establish a pore evolution model of the sandstone reservoir within a braided delta sedimentary system. This knowledge will not only shed new light on the reasons for the reservoir heterogeneity within the basin but also provide important new information for the exploration and development of this kind of reservoir all over the world.

## 2. Geological background

The Ordos Basin is located in the west of the North China platform and covers an area of ca. 25 × 104 km2 (Carroll et al., 2010; Xu et al., 2018). In contrast to the strong structural deformation at the margins of the basin, the internal structural deformation is extremely weak. Existing faults are not developed and the basin itself exhibits a gentle slope with dip angles of less than 1° (Fu et al., 2013). The Ordos Basin is composed of six first-rank tectonic units (Fig. 1): the Yimeng Uplift, the Weibei Uplift, the Jinxi Folded Belt, the Yishan Slope, the Tianhuan Depression, and the Western Edge Thrust Belt (Yang et al., 2019). The study area for this contribution is located in the south of the Ordos Basin, incorporating for instance the administrative districts of Huanxian, Yan'an, Fuxian, and Huating.

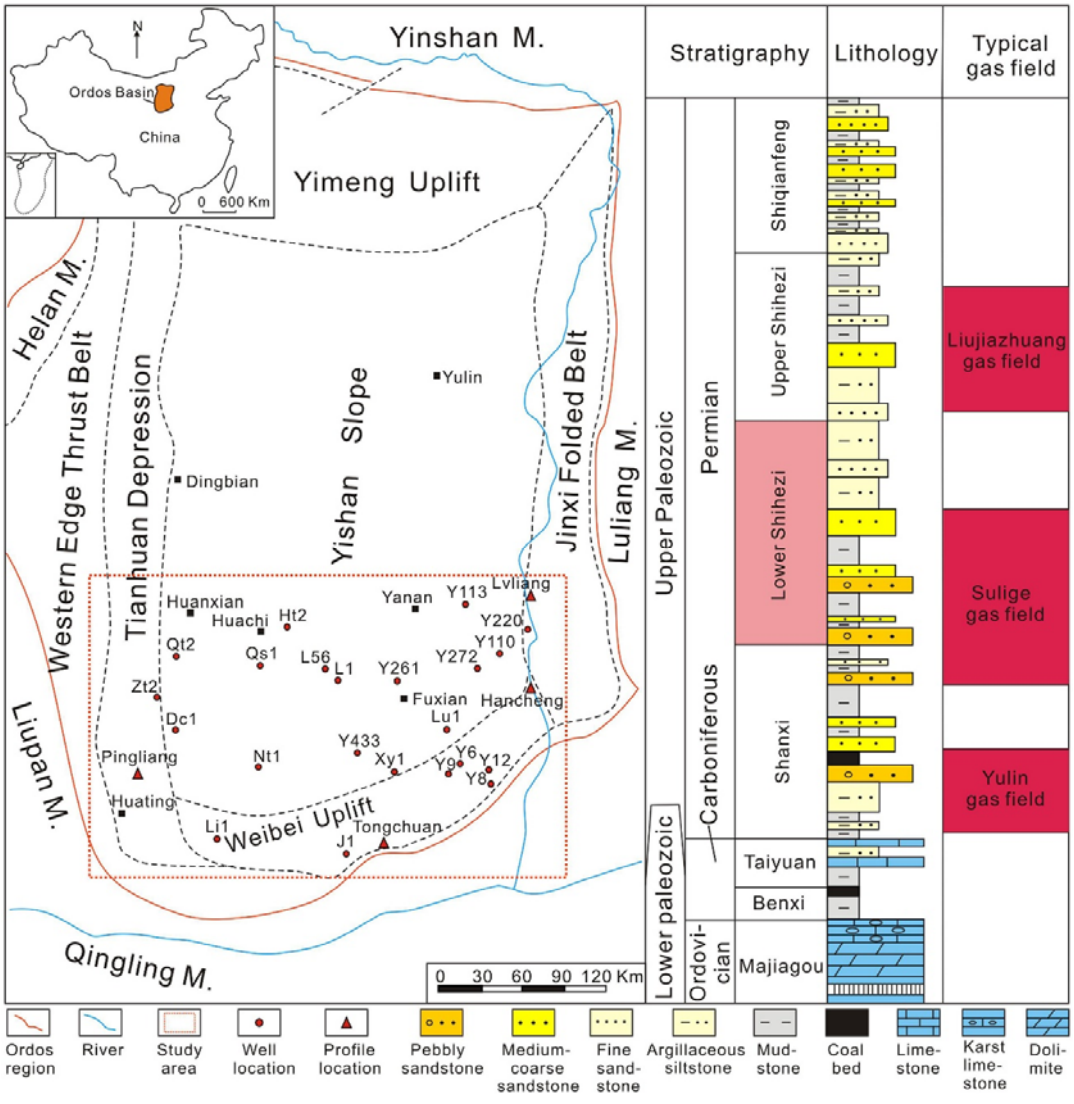


**Fig. 1**. Geographic location of the Ordos Basin and lithostratigraphic section of the Upper Paleozoic sedimentary sequences.

Modified from Jiu et al. (2021).

Upper Paleozoic sedimentary sequences are well developed within the Ordos Basin, consisting from base to top of the Carboniferous Benxi Formation and the Permian Taiyuan, Shanxi, Lower and Upper Shihezi, and Shiqianfeng formations (Fig. 1) (Xiao et al., 2019). The sedimentary thickness of the Lower Shihezi Formation ranges between 70 and 223 m. It is widely distributed throughout the basin and gradually increases in thickness from south to north. The sandstones of the Lower Shihezi Formation are relatively coarse. Nevertheless, the sandstone bodies represent a tight sandstone reservoir, which, regardless of the relatively low porosities and permeabilities, constitutes the main exploration target in the basin (Jiu et al., 2021).

## 3. Method of sample preparation and analysis

The logging data of 48 wells were gathered from the southern Ordos Basin. Furthermore, 4 field profiles and cores of 32 wells were recorded. The sedimentary facies types and their distribution were determined by analyzing the logging data, lithology and depositional structures.

In total, 180 thin sections were made at China University of Geosciences. Potassium ferricyanide and alizarin red were used for the purpose of distinguishing carbonate minerals more effectively. During this method, pure calcite is dyed red. If the calcite contains iron, it is dyed purple red. Iron-rich dolomite is dyed bright blue. A Zeiss optical polarization microscope was used to investigate the detrital, matrix and cement compositions by counting at least 300 points per thin section. Grain size information was obtained by averaging long-axis measurements of 300 grains per thin section (overgrowth of quartz and feldspar were not considered for grain size measurements) (Huang et al., 2020).

For the purpose of analyzing the pore types and their distribution, sixty casting thin sections were made (with red epoxy). Normal light microscopy was combined with scanning electron microscope (SEM) analysis to investigate the structure of pores and clay minerals. In order to avoid electron charging effects, the samples need to be coated with platinum and gold. After this treatment, a Phenom Pro scanning electron microscope was utilized for investigation.

339 samples were collected from 32 wells to describe and analyze the sedimentary lithofacies types. Altogether 2318 samples were measured for porosity and permeability from 48 wells in order to provide additional information on the reservoir characteristics of the different sedimentary facies. Porosity and permeability values were measured at the China Petrochemical Corporation. The measurements were carried out on a YRD-FKS-2 instrument under overburden pressure via nitrogen gas.

Seven sandstone samples were collected from 2 wells and tested for the maximum pyrolysis temperature (***. $T_{max}$***). Eight samples were collected from 4 wells and tested for the compositions of clay minerals. The above tests were carried out at the Changqing Oilfield Exploration and Development Research Institute. The experimental results were used as parameters to define diagenetic stages. ***. $T_{max}$*** values were obtained through a ROCK-EVAL 6 pyrolysis apparatus. The compositions of clay minerals were analyzed through (D/max-2500) X-ray diffraction (XRD).


**Fig. 2.** Core and field profile photos. (A) Pebbly sandstone, Pingliang profile; (B) low-angle cross-bedding, Pingliang profile; (C) trough cross-bedding, Tongchuan profile; (D) wedge cross-bedding; Pingliang profile; (E) siltstone with ripple cross-lamination, Y220 well, 3064.2 m; (F) siltstone with massive bedding, Y12 well, 2250.1 m; (G) siltstone with low-angle cross-bedding (black arrow), L1 well, 3364 m; (H) convoluted bedding, a kind of slump deformed structure, Pingliang profile; (I) massive mudstone, Y272 well, 2442.2 m; (J) carbonaceous mudstone, L1 well, 3465 m; (K) horizontal lamination, Tongchuan profile; (L) plant debris in mudstone (blue arrow), L1 well, 3425 m; (M) erosional basal surface (yellow dotted line), L1 well, 3466 m; (N) multiphase sandbody of distributary channel overlaps, Pingliang profile.

## 4. Results

### 4.1. Analysis of sedimentary characteristics

The Lower Shihezi Formation in the southern Ordos Basin mainly developed within a braided delta (which can be subdivided into braided delta plain and braided delta front) and shore shallow lake environment (cf., Li et al., 2016; Liang et al., 2018). Based on texture and sedimentary structures that

were obtained from the studied core samples and field profiles, several lithofacies types could be distinguished within the study area.

#### *4.1.1. Lithofacies types*

Within the study area, mainly sandstone facies, siltstone facies, and mudstone facies can be found, which can be subdivided into 11 lithofacies (Fig. 2).

The sandstone facies is mainly composed of gray to gray–green and light red coarse to fine sandstone, and can be subdivided into pebbly sandstone (Sp) (Fig. 2A), sandstone with low-angle cross-bedding (Sa) (Fig. 2B), sandstone with trough cross-bedding (St) (Fig. 2C), and sandstone with wedge cross-bedding (Sw) (Fig. 2D).

The siltstone facies is mainly composed of gray siltstone and argillaceous siltstone, and can be subdivided into siltstone with ripple cross-lamination (Fr) (Fig. 2E), massive siltstone (Fm) (Fig. 2F), siltstone with low-angle cross-bedding (Fa) (Fig. 2G), and slump deformed siltstone (Fsd) (Fig. 2H).

The mudstone facies is mainly composed of gray and grayish-black mudstone and silty mudstone, and can be subdivided into massive mudstone (M) (Fig. 2I), carbonaceous mudstone (Mc) (Fig. 2J), and mudstone with horizontal lamination (Mh) (Fig. 2K).

#### *4.1.2. Lithofacies associations*

Based on the depositional settings and well log curves (Fig. 3), the different lithofacies types can be grouped into 7 distinct lithofacies associations (lithofacies association A–H).

##### *4.1.2.1. Lithofacies association A (M-Mh-Mc)*

Lithofacies association A is mainly composed of grayish-black mudstone and gray silty mudstone, with thin layers of grayish-black carbonaceous mudstone. The rocks either appear massive or have a horizontal lamination developed. Fossils of plant fragments are common (Fig. 2L). The GR curve of lithofacies association A is tooth-shaped and exhibits high amplitudes (Fig. 3).

The mudstone in lithofacies association A was most probably deposited between distributary channels of a river system. The carbonaceous mudstone, horizontal lamination and plant fragments indicate a reducing environment. The high GR values indicate high clay contents (Nazeer et al., 2016; Li et al., 2010; Cheng et al., 2020). Thus, lithofacies association A may be interpreted as an interdistributary swamp.

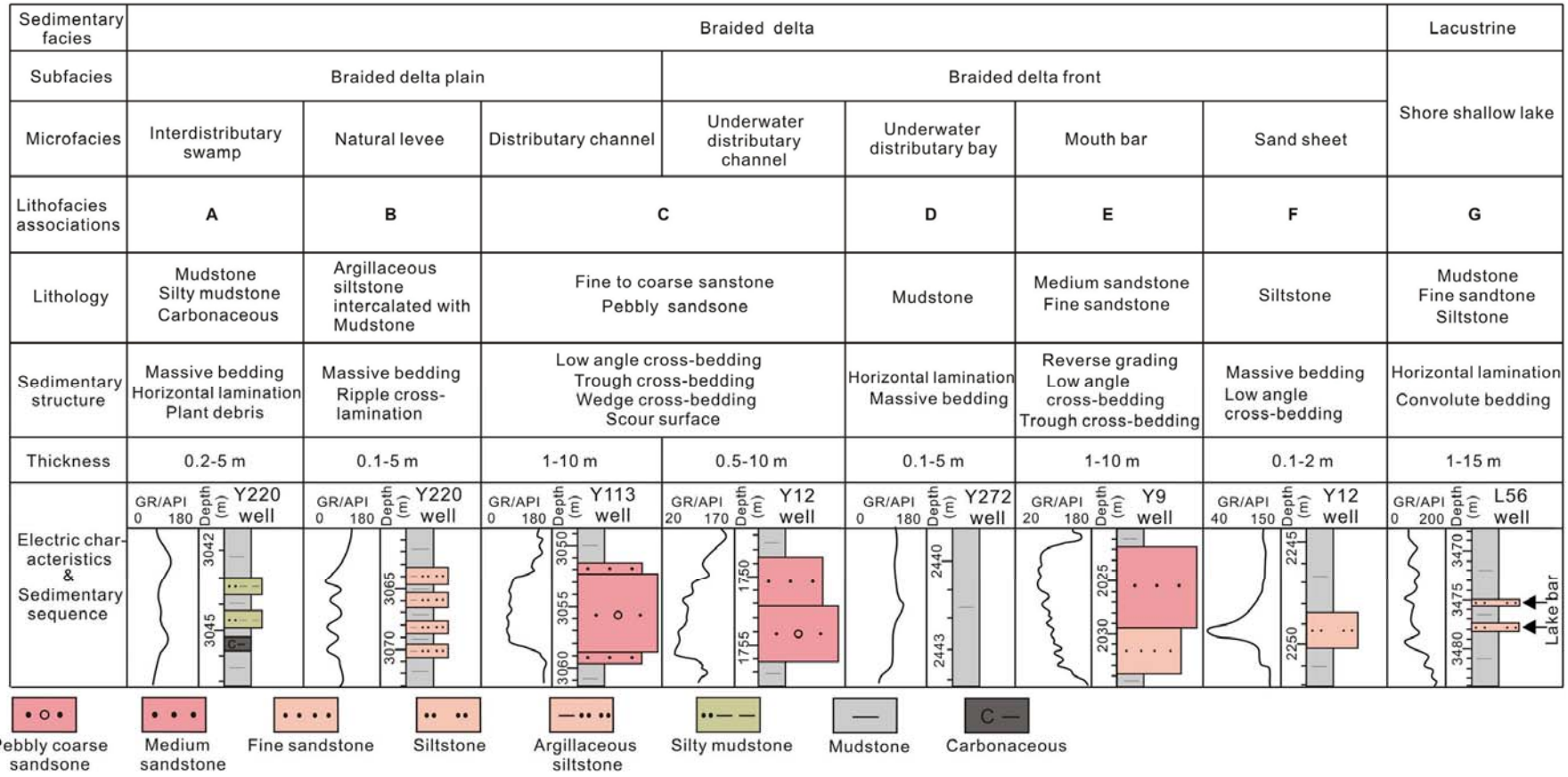


**Fig. 3**. Description of facies recognized in the study area.

*4.1.2.2. Lithofacies association B (Fr-M)*

Lithofacies association B is characterized by gray massive mudstone, and ripple cross-laminated gray mudstones and argillaceous siltstones, The mudstones and argillaceous siltstones are interbedded with thicknesses of single layers of <5 m. The GR logging curves are mostly serrated (Fig. 3).

Thin layers of siltstone interbedded with mudstone are mainly formed as a response to flood events between distributary channel deposits in a delta plain. The ripple cross-lamination may reflect the turbulent water conditions during floods. The serrated GR logging curve commonly reflects frequent changes in clay content (Nazeer et al., 2016). Thus this lithofacies association can be interpreted as the deposits of natural levees.

*4.1.2.3. Lithofacies association C (Sp-Sa-St-Sw)*

Lithofacies association C is characterized by gray to gray–green and light red fine to coarse sandstones, and pebbly sandstones. All deposits can be trough cross-bedded, wedge cross-bedded, or low-angle cross-bedded. The lower boundaries to the underlying lithofacies are often erosional (Fig. 2M). The thicknesses of single layers range from 0.5 to 10 m. Multiphase sandbody overlaps are common (Fig. 2N). The natural gamma-ray (GR) curve is box-shaped or bell-shaped (Fig. 3).

Among all lithofacies associations, lithofacies association C exhibits the coarsest grain sizes. The presence of trough cross-bedding, wedge cross-bedding, and low-angle cross-bedding indicates changes in the fluvial depositional processes during the migration of dunes. The bell-shaped logging curve may reflect the migration of the channel. Therefore, lithofacies association C is interpreted as having developed within an (underwater) distributary channel.

*4.1.2.4. Lithofacies association D (M-Mh)*

Lithofacies association D is dominated by dark mudstones. Massive bedding and horizontal lamination are common. The deposits of this lithofacies association can mostly be encountered in between the deposits of lithofacies association C (underwater distributary channels). The GR curve is tooth-shaped (Fig. 3).

The dark color of the rocks may point to a reducing depositional environment. The massive bedding to horizontal lamination points to deposition via suspension settling. In general, lithofacies association D can be interpreted as the deposits formed within an underwater distributary bay.

*4.1.2.5. Lithofacies association E (Sa-St)*

Lithofacies association E is less common within the study area and is dominated by gray fine to medium sandstones. Often, the sandstones show reverse grading and low-angle cross-bedding to trough cross-bedding. The thickness of the sandbodies may range between 1 and 10 m. The corresponding GR of this lithofacies association is funnel-shaped (Fig. 3).

The reverse grading of this lithofacies association can be explained by progradation into the lake basin and the decrease of flow velocity upon arrival of the fluvial sediment into the basin (Martini and Sandrelli, 2015). Therefore, we interpret lithofacies association F as the deposits of a mouth bar.

*4.1.2.6. Lithofacies association F (Fm-Fa)*

Lithofacies association F is characterized by well-sorted gray siltstones. The siltstones may be massive or show low-angle cross-bedding. Single bed thicknesses range between 0.1 and 2 m. This lithofacies association migrates laterally and is widely distributed at the delta front. Furthermore, the GR curves are finger-shaped with medium amplitude (Fig. 3).

Lithofacies association F can be interpreted as the deposits of sand sheets. Due to the strong transformation and redistribution of the estuary by waves and coastal currents, lithofacies association F can be widely distributed. The strong scouring action of waves and coastal currents led to a good degree of sorting (Li et al., 2010; Cheng et al., 2020).

*4.1.2.7. Lithofacies association G (M-Mh-Fsd)*

Lithofacies association G is mainly composed of dark gray mudstone with massive bedding and horizontal lamination, which is intercalated by 0.5–1 m gray siltstones and fine sandstones. Slump deformation structures are common. The GR logging curve of this lithofacies association is mostly serrated and exhibits high values (Fig. 3).

The dark color of these rocks may indicate a reducing environment. Due to the massive bedding to horizontal lamination, it can be assumed that deposition took place through suspension settling. The abundant deformation structures can be explained by the collapse of unconsolidated sediments at the delta front due to seismic activity (Jiang et al., 2010). Therefore, lithofacies association G can be interpreted as having formed in a shallow lacustrine environment.

***4.1.3. Sedimentary facies distribution***

Based on the drilling data and previous studies on provenance, the studied sediments can be assumed to have originated from the south and north (Li et al., 2016; Ma et al., 2016; Liang et al., 2018). A fence diagram of the Lower Shihezi Formation was created to illustrate the sedimentary facies distribution (Fig. 4). During the time of Lower Shihezi Formation deposition, two main provenance areas provided the necessary clastic material, the Yinshan Mountain in the northeast, and the Qinling Mountain in the South (Ma et al., 2016; Liang et al., 2018). In consequence, two braided deltas developed under the influence of the two provenance areas. Within the study area, the Lower Shihezi Formation is primarily dominated by the sedimentary rocks that formed in braided delta front and braided delta plain environments. The largest sandbodies belong to the distributary channels and underwater distributary channels that also exhibit the coarsest grain sizes. The sand sheet microfacies is well developed, but corresponding sandbodies are relatively thin. The deposits of the mouth bar microfacies are only developed locally.

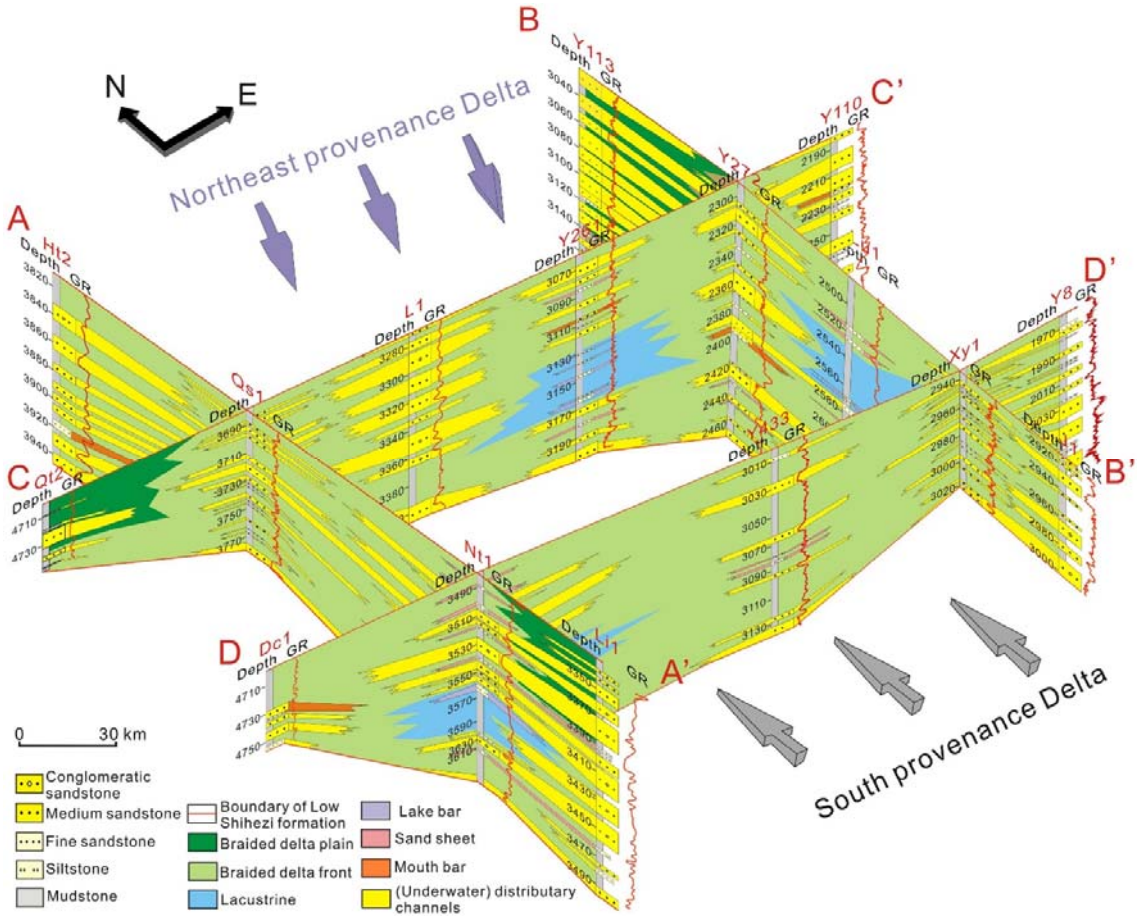


**Fig. 4.** Fence diagram show the spatial distribution of braided deltas and lacustrine facies of the Lower Shihezi Formation.

Based on well analysis and fence diagram analysis, a sedimentary facies map of the Lower Shihezi Formation in the southern Ordos Basin can be made (Fig. 5). As can be seen from the distribution of the different lithofacies types, during the development of the Lower Shihezi Formation, the largest part of the study area was occupied by a braided delta, and only a small area in the center and the north of the study area was covered by (a) lake(s). The underwater distributary channels are presented in form of larger lenses whereas the interdistributary swamps and underwater distributary bays are located on both sides of the channels. Sand sheets are distributed at the front of a delta.

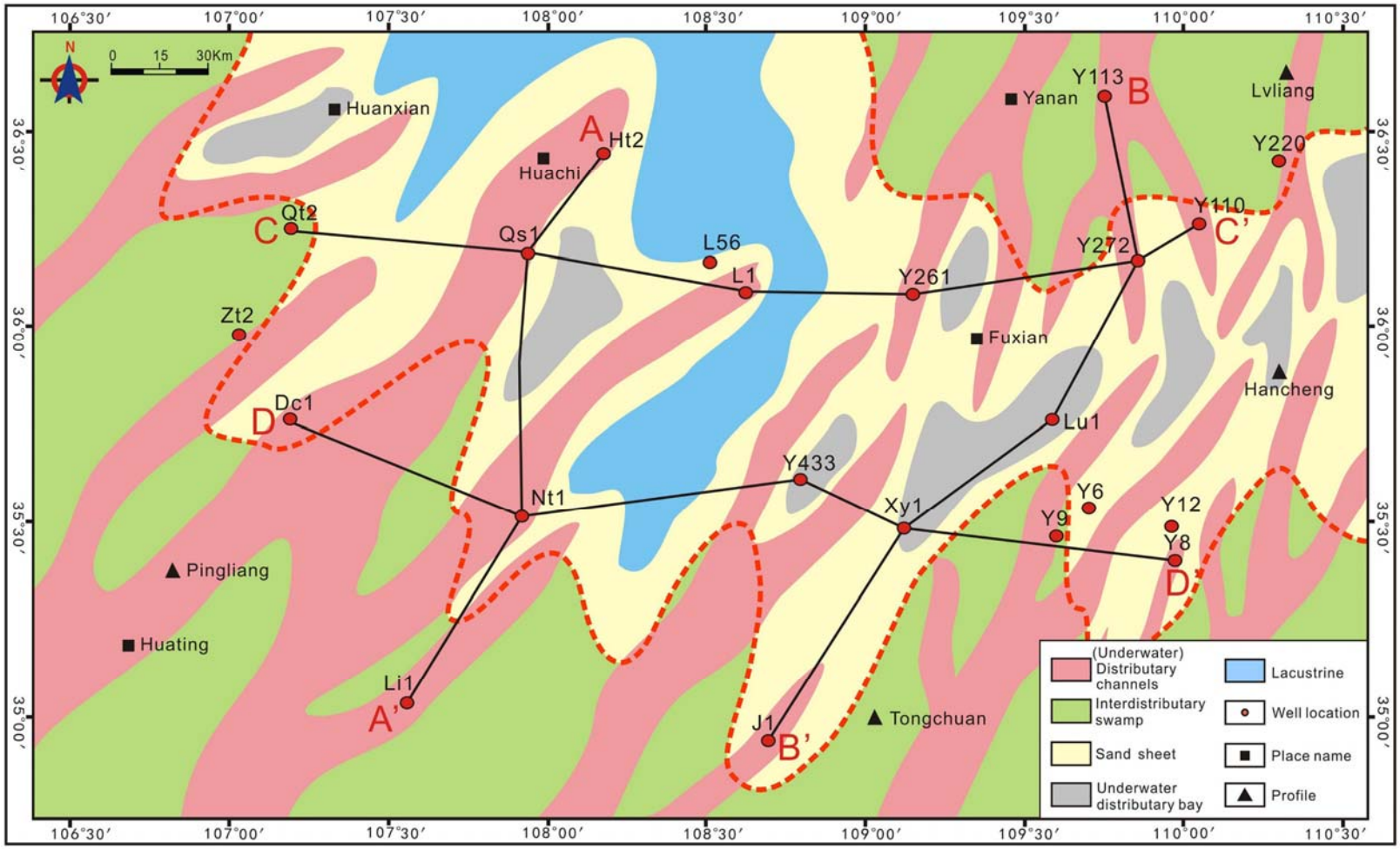


**Fig. 5**. Sedimentary facies map of the Lower Shihezi Formation in the study area.

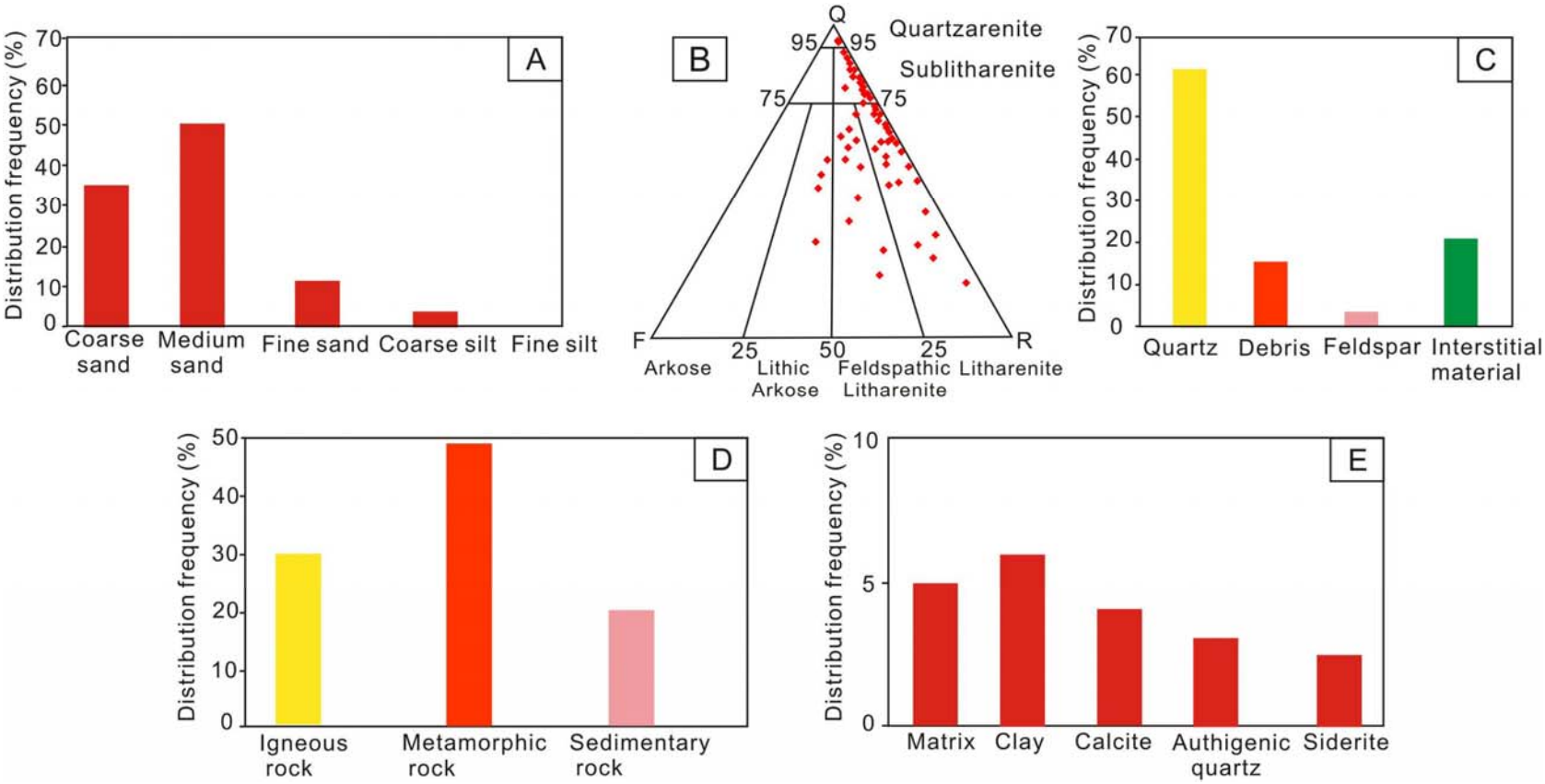


**Fig. 6**. (A) Grain size features of the sampled sandstones; (B) QFR diagram of the detrital compositions of the Lower Shihezi Formation (after Folk, 1980); (C) sandstone component histogram; (D) rock fragments component histogram; (E) filler component histogram.

### 4.2. Reservoir characteristics

#### *4.2.1. Petrologic characterization of the reservoir*

As previously mentioned in Section 4.1.1, the reservoirs of the Lower Shihezi Formation are mainly characterized by medium to coarse sandstones, fine sandstones, and siltstones (Fig. 6A). The roundness of the particles varies from angular to sub-angular. All analyzed rocks are grain-supported with concavo-convex and sutured contacts between particles, and exhibit compact filling (Fig. 7A–D). The analyzed samples can predominantly be classified as litharenites and sublitharenites, followed by feldspathic litharenites, and a few quartzarenites and lithic arkoses (Fig. 6B). The clastic composition (vol%) of the sandstones is dominated by quartz (60.3% on average). The contents of feldspar and rock fragments are relatively small, with an average of 15.2% and 3.5%, respectively (Figs. 6C and D).

The rock fragments mainly consist of particles originating from metamorphic rocks (on average 49%), such as phyllite (Fig. 7C), quartzite (Fig. 7D), schist, and slate. In addition, magmatic (average content of 30%) and sedimentary rock fragments (average content of 19%) can be found.

The pore spaces between the sand grains are mainly filled by cement and matrix, forming between 5 and 35% (on average 21%) of the whole volume of the rock. Among the types of cement, the content of clay cement is the highest, with an average of 6.5%, followed by calcite cement (4.2%), authigenic quartz (3.6%), and siderite cement (1.7%). The content of other types of cement is relatively low (<1%) (Fig. 6E).

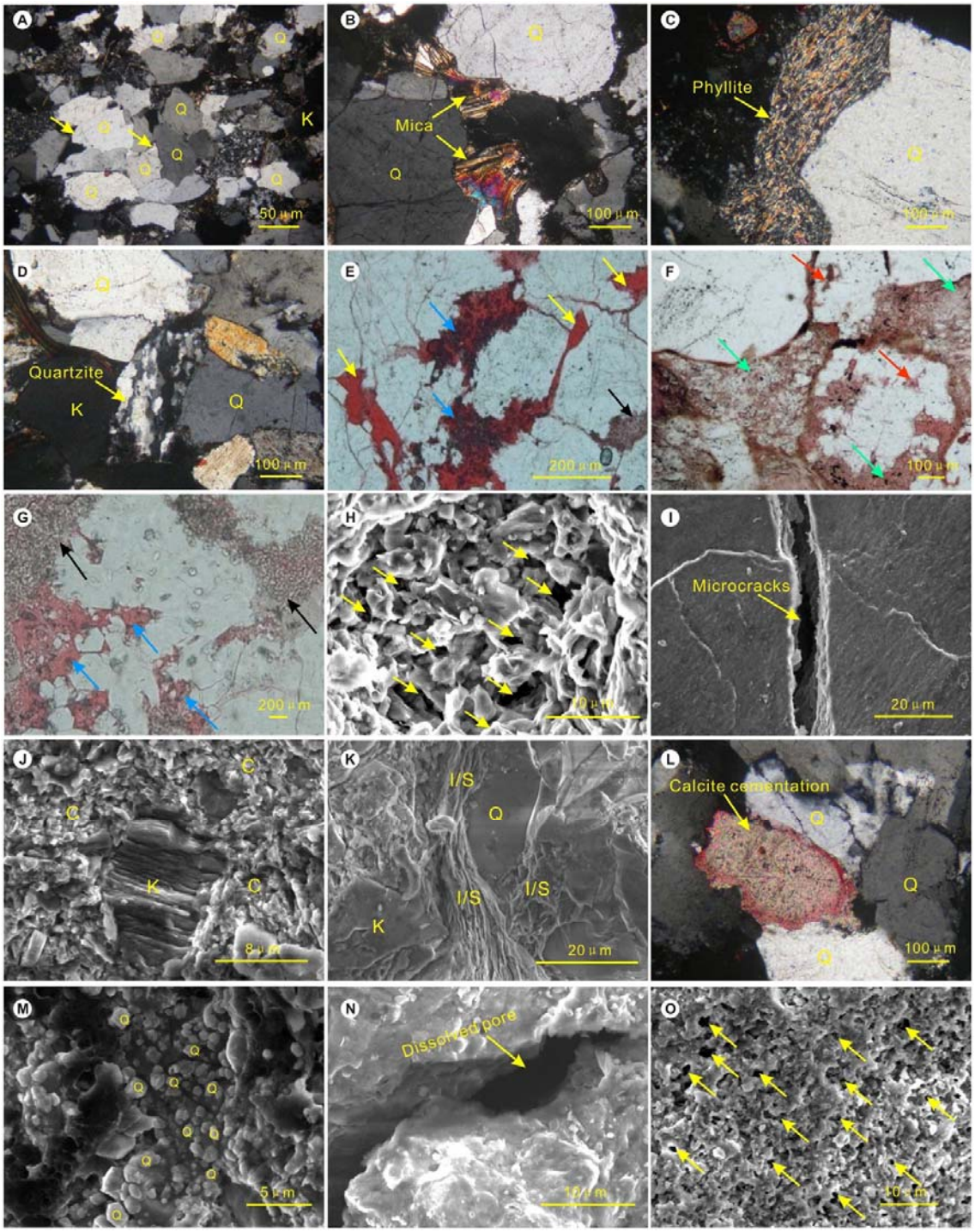


**Fig. 7.** Photomicrographs and SEM images. (A) The clastic grains are in point to line contact, with authigenic quartz (yellow arrow), Pingliang profile; (B) mica is extruded and deformed (yellow arrow), Pingliang profile; (C) phyllite is deformed by compaction (yellow arrow), Tongchuan profile; (D) quartzite (yellow arrow), Pingliang profile; (E) intergranular dissolution pores (blue arrow) and residual intergranular pores (yellow arrow), Zt2 well, 5032 m; (F) rock fragments dissolution pores (green arrow) and feldspar dissolution pores (red arrow), Y6 well, 2148 m; (G) intergranular dissolution pores (blue arrow) and intercrystal pores (black arrow), Qt2 well, 4729 m; (H) intercrystal pores (yellow arrow), L1 well, 3315 m; (I) microcracks (yellow arrow), L1 well, 3360 m; (J) pores filled with chlorite, L1 well, 3311 m; (K) pores filled with illite mixed layers, L1 well, 3363 m; (L) calcite cementation (yellow arrow), Pingliang profile; (M) authigenic microcrystalline quartz occurs

in the form of coating, L1 well, 3311 m; (N) dissolution pore (yellow arrow), L1 well, 3365 m; (O) pores were formed by the dissolution of matrix, L1 well, 3363 m. Q = quartz; K = k-feldspar; C = chlorite; I/S = illite–smectite mixed layers.

#### *4.2.2. Characteristics of reservoir properties*

The porosities of the Lower Shihezi Formation sandstone are very low (5.74% on average), ranging from 0.66% to 12.89%. The peak porosity is 4–6% (Fig. 8A). The measured permeabilities are between 0.01 × 10−3 μm2 and 2.44 × 10−3 μm2 with an average value of 0.26 × 10−3 μm2. The peak permeability is 0.1 × 10−3 μm2 to 0.5 × 10−3 μm2 (Fig. 8B). It is interesting to note that there is a positive correlation between the reservoir porosity and the permeability in the studied samples (Fig. 8C).

#### *4.2.3. Pore types*

The study of the pores of the sampled material shows that intergranular pores, dissolution pores, and intercrystal pores are the main pore types that can be observed, followed by microfractures (Fig. 8D).

Residual intergranular pores are formed when the original intergranular pores are filled with chlorite, calcite, kaolinite, etc. They are relatively well developed in quartz sandstone and lithic quartz sandstone within the study area, showing irregular polygons (Fig. 7E), with pore diameters of 20–70 μm.

Dissolution pores are the most common pore type in the analyzed samples and can be subdivided into intragranular dissolution pores and intergranular dissolution pores. The pore diameters of this pore type are relatively small and generally less than 50 μm. The intragranular dissolution pores are mainly formed by the local dissolution of rock debris and feldspar during diagenesis (Fig. 7F). On the other hand, during diagenesis, intergranular dissolution pores can be formed by the dissolution of pore-filling material (calcite cement, clay cement, etc.) (Fig. 7G).

Intercrystal pores are mainly formed by alteration and hydration of feldspar and cuttings, and recrystallization of argillaceous matrix between grains (Fig. 7G and H). Although the diameters of these pores are generally small (1–10 μm), this pore space type is relatively important within the study area.

Finally, microfractures are also relatively common in the analyzed samples. The fractures are small and narrow, exhibiting widths of 10–20 μm. Despite only accounting for 3% of the total porosity of the reservoir, the microfractures may improve the reservoir permeability within the study area.

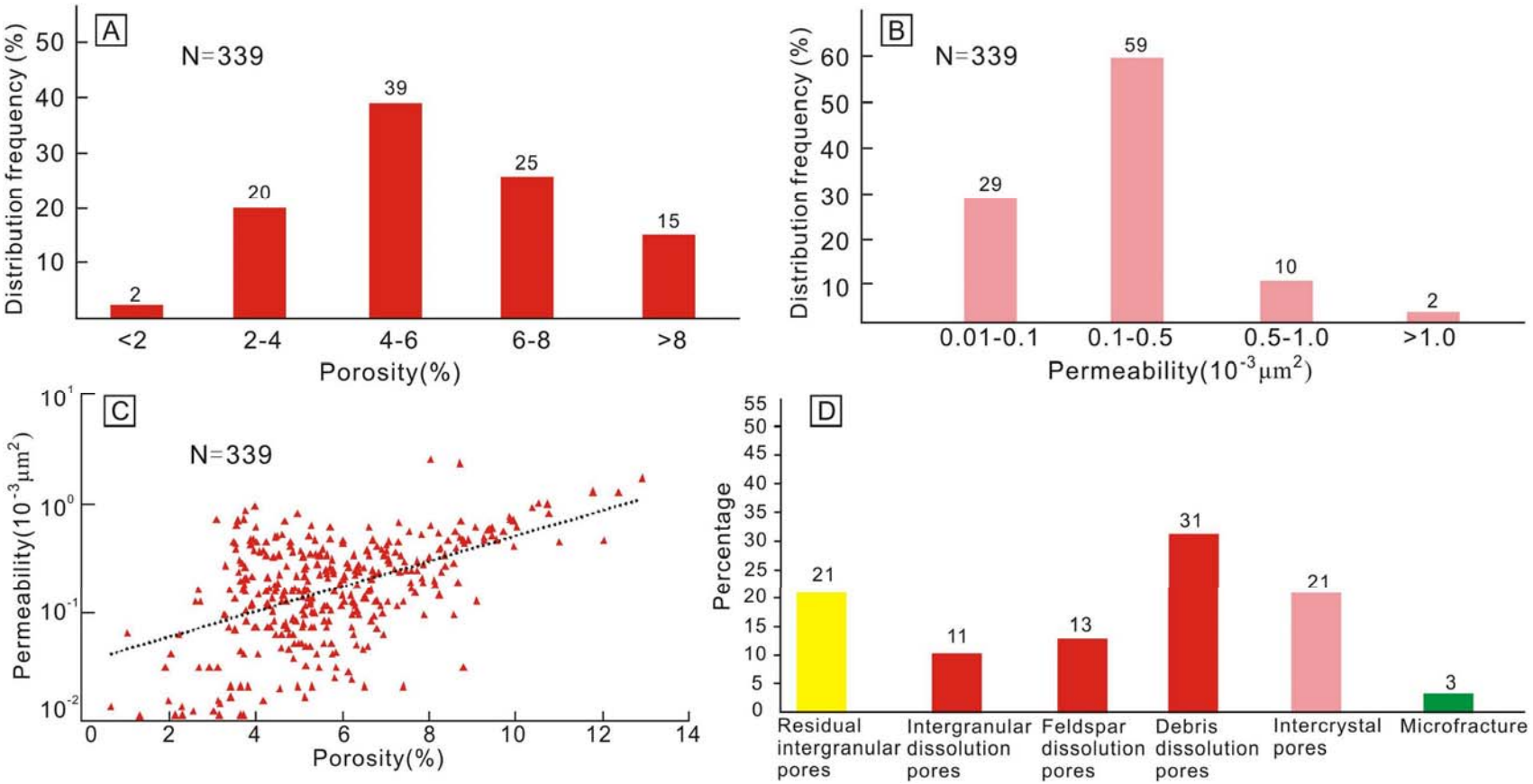


**Fig. 8.** (A) Histogram of the porosity distribution; (B) histogram of the permeability distribution; (C) plot relationship showing porosity is positively correlated with permeability; (D) histogram of pore type distribution.

#### *4.2.4. $T_{max}$ values and relative content of clay minerals*

The ***. $T_{max}$*** analysis on 8 samples shows values between 438 and 486 °C. Clay mineral analysis on 7 samples (Table 1) indicates that the clay minerals in the Lower Shihezi Formation are dominated by illite, followed by slightly lower contents of kaolinite and chlorite. Subordinately, illite/smectite mixed layers can be found.

**Table 1**. Relative content of clay minerals and smectite (S) in illite/smectite (I/S).

| Well | Depth | Illite | Kaolinite | Chlorite | I/S | S (%) |
|---|---|---|---|---|---|---|
| TS1 | 2286 | 28.3 | 42.3 | 12.8 | 16.7 | 10 |
| TS1 | 2287 | 14.6 | 20.8 | 61.8 | 2.8 | 10 |
| LC1 | 3100 | 47.7 | 12 | 17.5 | 22.8 | 5 |
| LC1 | 3101 | 45.6 | 31.8 | 14.2 | 8.4 | 5 |
| LC1 | 3103 | 55.6 | 18.1 | 13.2 | 13.1 | 5 |
| LC1 | 3104 | 47.6 | 19.3 | 13.8 | 19.4 | 10 |
| S2 | 1178 | 14 | 28.7 | 55.5 | 1.7 | 5 |
| T1 | 2224 | 47.7 | 36.5 | 12.3 | 3.5 | 10 |

## 5. Discussion

### 5.1. Diagenetic evolution

The processes during diagenesis and their different stages strongly affect the pore characteristics and therefore affect the quality of a reservoir (Stonecipher et al., 1984; Y. Li et al., 2021; Ma et al., 2021). So far, several geologists studied the diagenetic stage(s) of the Lower Shihezi Formation in the south of the Ordos Basin and concluded that this formation entered the mesodiagenetic stage (A and B) (Zhang et al., 2009; S. Li et al., 2021; Zhang et al., 2021). To correctly define the diagenetic stages of the rocks within the study area, the contact relationships between particles (Qian et al., 2020), assemblages and relative content of clay minerals (Y. Li et al., 2021; Su et al., 2021), and the characteristics of the different types of cement (Su et al., 2021) were studied. In addition, the measured ***. $T_{max}$*** values (Madec and Espitalie, 1984) and the smectite content in illite/smectite layers (Zhang et al., 2021) were used as further evidence for the characterization of a diagenetic stage.

Suture line contacts are relatively common in between the sedimentary grains of the Lower Shihezi Formation rocks. Quartz outgrowth is ubiquitous. Carbonate minerals are mainly spar calcite. According to China's criteria (SY/T 5477–2003), the ***. $T_{max}$*** values of the mesodiagenetic stage A are between 435 and 460 °C, and the contents of S range between 15 and 50%. The ***. $T_{max}$*** values of the mesodiagenetic stage B are between 460 and 490 °C, and the S contents are <10%.

The ***. $T_{max}$*** and clay mineral analyses on our samples show that the ***. $T_{max}$*** values range between 438 and 486 °C. The corresponding S contents are <10% (Table 1). All these phenomena support the hypothesis that the Lower Shihezi Formation entered the A and B stages of mesodiagenesis and therefore agree with the previous studies mentioned above (Fig. 9).

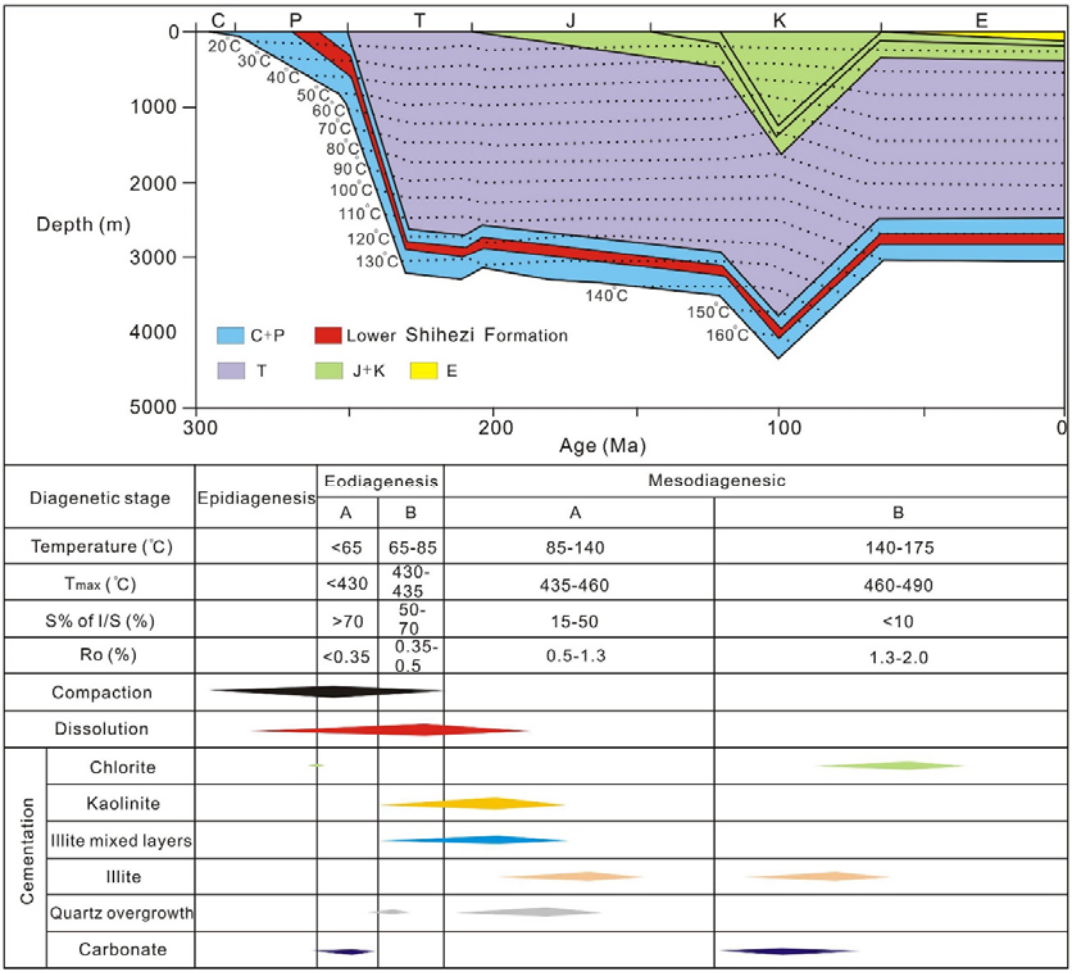


**Fig. 9.** Burial and thermal history and paragenetic sequence of the southern Ordos Basin.

Modified from S. Li et al. (2021).

### 5.2. Diagenetic control on the reservoir

According to our observations, compaction, cementation, and dissolution have the greatest influence on reservoir quality.

#### *5.2.1. Compaction*

The sandstone grains within the studied samples mainly exhibit linear contacts with local suture line contacts. The observed mica, rock fragments, and other plastic particles appear bent and deformed (Fig. 7C). All this demonstrates that the Lower Shihezi Formation went through strong compaction. Mechanical compaction generally destroys the original pore space, which may reach a degree of damage of 25–80% within the studied samples (Fig. 10A). Therefore, except for a few samples in which pore space reduction is due to cementation (in the rectangle of Fig. 10A), the pores of most samples are reduced by compaction. The degree of compaction generally increases with an increase in burial depth and thereby, in turn, leads to a decrease in the physical reservoir properties (Fig. 11).

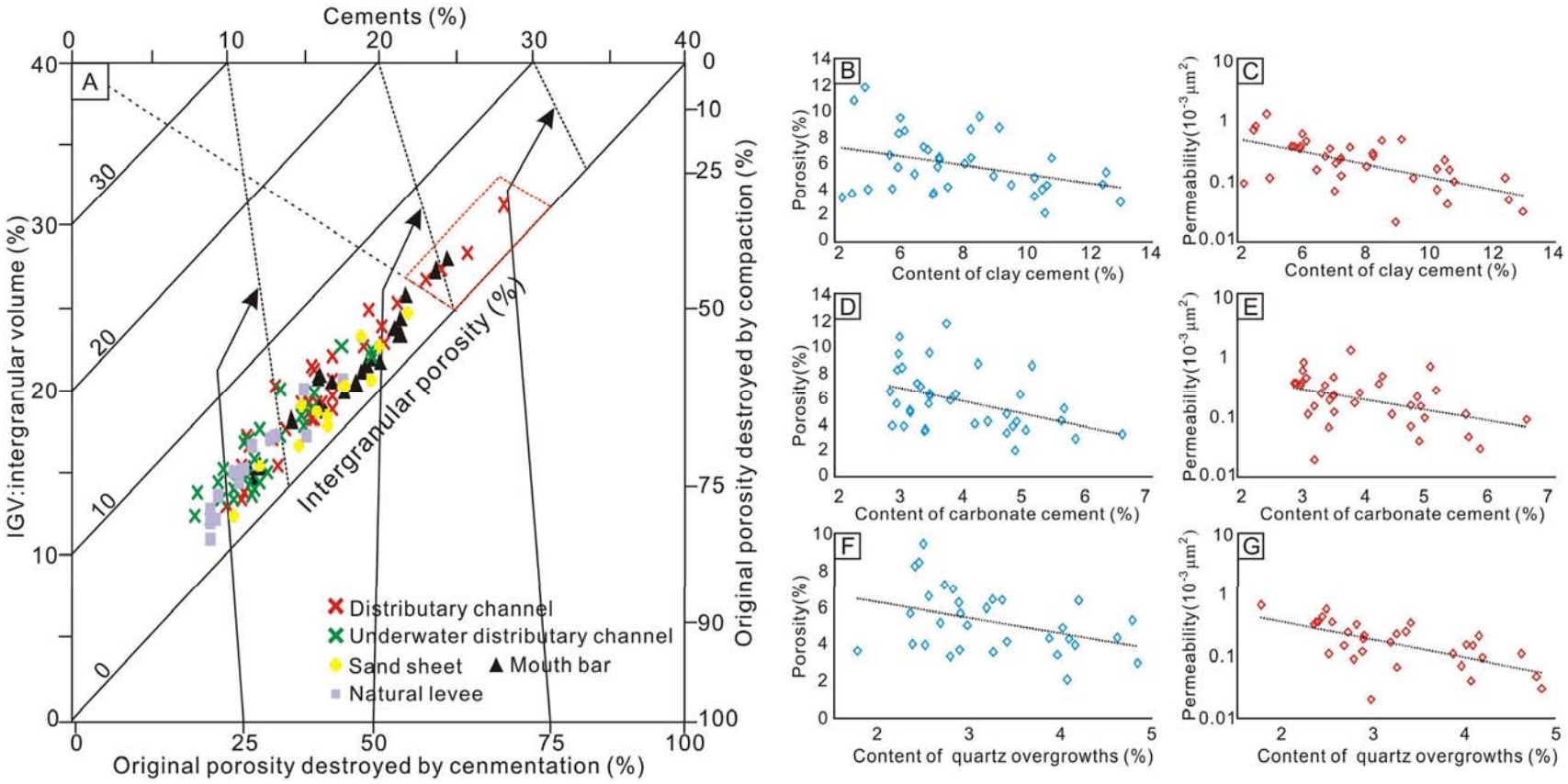


**Fig. 10.** (A) Relationship between the volume of intergranular cement and the total intergranular volume (after Ehrenberg, 1989). (B) and (C) Plot relationship showing the correlation between clay mineral cement content and porosity/permeability of the Lower Shihezi Formation. (D) and (E) Plot relationship showing the correlation between carbonate cementation content and porosity/permeability. (F) and (G) Plot relationship showing the correlation between quartz overgrowth content and porosity/permeability.

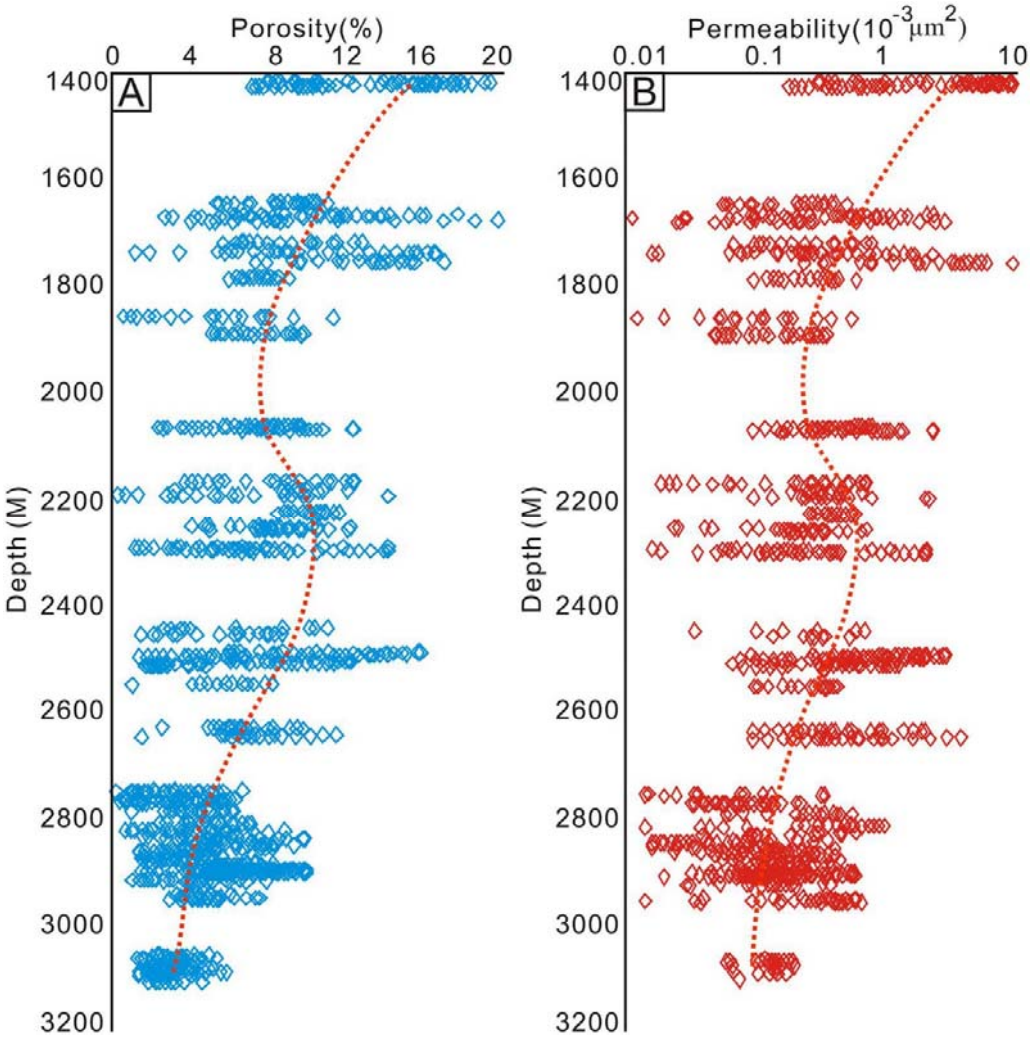


**Fig. 11.** (A) Plot relationship showing porosity varies with depth of the Lower Shihezi Formation; (B) plot relationship showing permeability varies with depth of the Lower Shihezi Formation.

### *5.2.2. Cementation*

Cementation can destroy the original pores and reduce the reservoir quality (Dutton, 2008). There are three types of cementation within the study area: (1) siliceous cementation, (2) calcareous cementation, and (3) authigenic clay mineral cementation.

The content of authigenic clay mineral cement is the highest in the samples with mainly kaolinite, chlorite, montmorillonite, and illite mixed layers. The clay minerals mainly occur in the form of pore filling and pore lining filling (Fig. 7J and K). Pore filling of cement commonly blocks the pore and throat, reducing the pore throat connectivity and intensifying the densification process (Ehrenberg, 1989). A negative correlation can be observed between the clay cement content and the physical properties of the analyzed sandstones (Fig. 10B and C), indicating that clay cementation has a destructive impact on reservoir quality.

Within the study area, carbonate cement is mainly made up of calcite. Early calcite mainly developed in an alkaline pore water environment, with floating particles and basal cementation (Liu et al., 2014), which is rare in the study area. The late calcite cementation mainly occurred at the B stage of mesodiagenesis, and the intergranular pores were often filled sporadically (Fig. 7L), which reduced the physical properties of the reservoir. A clear negative correlation can be observed between carbonate cement content and sandstone porosity (Fig. 10D and E). Therefore, high contents in carbonate cement are not helpful to the formation of a good reservoir.

Siliceous cementation is mainly characterized by quartz overgrowth (Fig. 7A) and authigenic microcrystalline quartz (Fig. 7M). This study found that the strength of quartz overgrowth increases with depth, and reaches its maximum at ca. 3500 m. The quartz overgrowth fills the pores and may completely occlude the pore space, showing the negative effects on the formation of high-quality reservoirs. Within the study area, there is a negative correlation between quartz overgrowth content and reservoir quality (Fig. 10F and G). Authigenic microcrystalline quartz is mainly formed by the dissolution of feldspar and rock fragments (J. Li et al., 2021). In the studied samples, the authigenic microcrystalline quartz generally occurs in the form of coating (Fig. 7M). Although the quartz overgrowth is destructive to the deep sandstone reservoir, under certain circumstances, the coating of microcrystalline quartz may have a protective effect on the primary intergranular pores (cf., Li and Hu, 2014).

#### *5.2.3. Dissolution*

Groundwater can dissolve rock components and improve the reservoir quality (Crundwell, 2014). In the studied samples, the soluble components among clastic particles, matrix, and cement have been dissolved in varying degrees to form secondary pores (Fig. 7N and O). With progressing diagenesis, early compaction and cementation will lead to a continuous decline of the physical reservoir properties. At the depth of 2000–2500 m, however, secondary pores are formed due to dissolution. This may be due to the organic matter within the source rocks of the Shanxi Formation, which started to mature and decarboxylate during burial (Y. Li et al., 2021), eventually leading to a significant increase in porosity and permeability (Fig. 11).

### 5.3. Influence of sedimentary facies on sandstone reservoir quality

The quality of a sandstone reservoir strongly depends on the environmental conditions in which it initially formed and which determines the composition and content of clastic particles, their degree of sorting and rounding, as well as the composition of matrix and cement. The sandstones of the Lower Shihezi Formation are mainly distributed in (underwater) distributary channels, natural levees, mouth bars, and sand sheets, while the lake sediments are mainly characterized by fine-grained mudstones. Therefore, the sandstone samples of 5 microfacies (distributary channel, underwater distributary channel, natural levee, mouth bar, and sand sheet) were selected for physical property analysis and comparison.

### *5.3.1. Control of clastic grain composition and grain size on sandstone reservoir*

The composition of clastic grains has distinctive effects on the physical reservoir properties (Y. Li et al., 2021). Within the studied samples, quartz is the most important mineral, which has a strong anti-compaction ability and can protect the pores during compaction (Crundwell, 2014). Our observations show that the quality of the physical properties of the reservoir increases together with an increase in quartz content (Fig. 12A and B). During diagenesis, the rock fragments may dissolve and form secondary pores, which will increase the physical properties of the reservoir. However, the rock fragments are easy to squeeze into the pores during compaction, which will reduce the reservoir quality (Y. Li et al., 2021). Within the study area, the content of rock fragments is therefore negatively correlated with the physical reservoir properties (Fig. 12C and D), indicating that the ability of secondary pores produced by rock fragments dissolution is limited. Consequently, rock fragments are strongly affected by compaction, which may lead to a decrease in pore space. Similar to quartz, feldspar particles also exhibit anti-compaction abilities, even though not as good as quartz particles (Li et al., 2011; Zhang et al., 2016). Nevertheless, feldspar can develop quite a lot of intragranular dissolved pores in the process of diagenesis. In the studied samples, however, the feldspar content is very low and thereby has only little influence on the reservoir.

In addition, to the composition of clastic grains, the grain size itself is also an important factor that may influence the development of the reservoir quality (Yu et al., 2020; Y. Li et al., 2021). Our observations provide evidence that the quality of the physical reservoir properties increases with larger grain sizes (Fig. 12E and F). For instance, the average porosities of coarse-grained sandstone, medium-grained sandstone, fine-grained sandstone, and siltstone are 9.81%, 7.13%, 5.36%, and 3.22%, respectively. Corresponding permeabilities (on average) are $0.72 \times 10{-}3$ μm2, $0.47 \times 10{-}3$ μm2, $0.35 \times 10{-}3$ μm2 and $0.28 \times 10{-}3$ μm2, respectively.

### *5.3.2. Impact of matrix content on sandstone reservoir*

In general, the matrix fills the gaps in between the larger sedimentary particles, which is not conducive to the rate of flow of pore fluid. Therefore, in a reservoir that exhibits relatively low amounts of a matrix, the flow space for pore fluids is larger. This, in turn, may be conducive to the occurrence of dissolution and eventually the generation of dissolution pores (Y. Li et al., 2021). A further negative effect of the matrix on the reservoir properties is its plasticity. During compaction, it may be squeezed into primary pores and thus lead to a reduction in reservoir quality. This can be seen by a negative correlation between the content of the matrix and the physical reservoir properties (Fig. 12G and H).

### *5.3.3. Sandstone reservoir quality of different braided delta microfacies*

The results of this study show that all the different microfacies of the described braided deltas exhibit their unique reservoir properties (Table 2; Fig. 13). Differences between the microfacies are mainly caused by the variable amounts of quartz and rock fragments, the grain size, and the matrix contents.

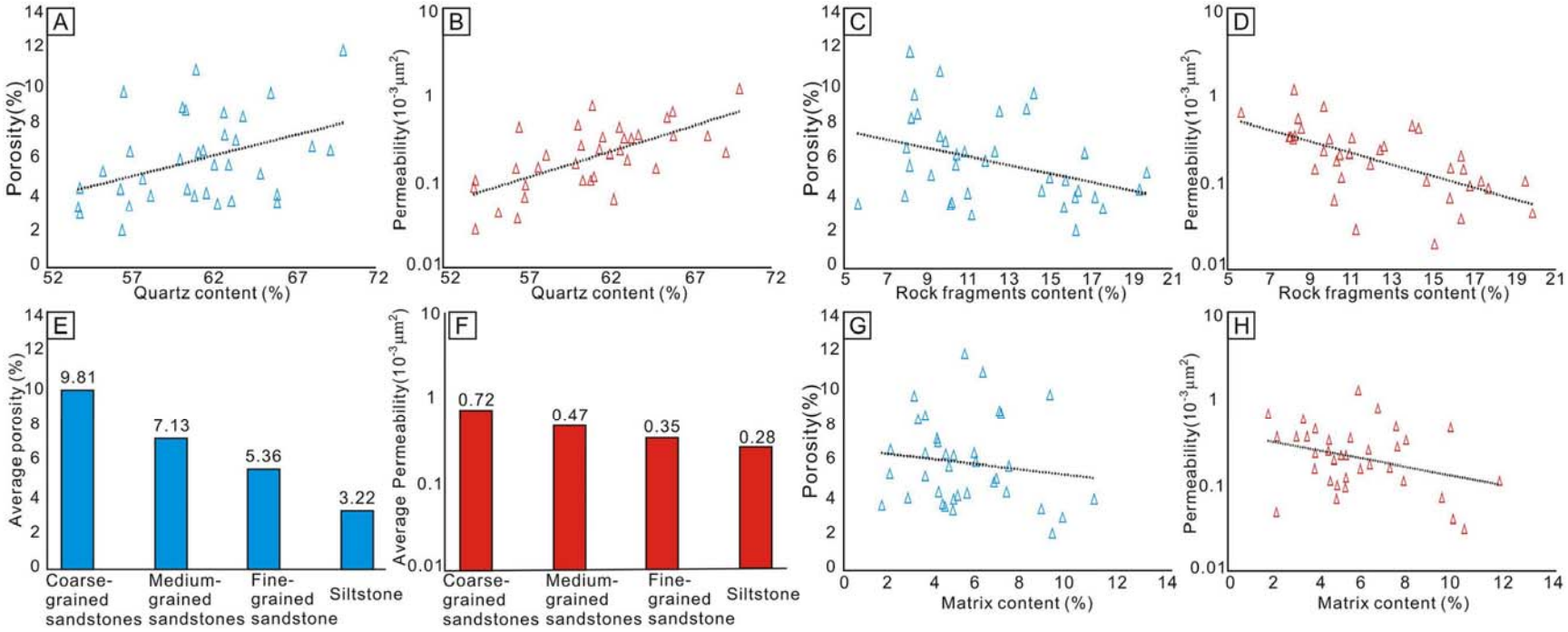


**Fig. 12.** (A) and (B) Plot relationship showing the relationship between quartz content and physical properties of reservoir; (C) and (D) plot relationship showing the correlation between rock fragments content and physical properties of reservoir; (E) and (F) histogram showing the correlation between grain sizes and physical properties of reservoir; (G) and (H) plot relationship showing the correlation between matrix content and physical properties of reservoir.

**Table 2.** Statistics of porosity and permeability of each sedimentary microfacies of Lower Shihezi Formation in the study area.

| Sedimentary microfacies | Distributary channel | Underwater distributary channel | Mouth bar | Sand sheet | Natural levee |
|---|---|---|---|---|---|
| Porosity (%) | 2.61 – 12.89 / 5.94 | 1.04 – 10.98 / 6.06 | 2.67 – 8.22 / 5.08 | 1.92 – 7.84 / 4.70 | 0.66 – 5.29 / 3.24 |
| Permeability ($10^{-3}$ μm$^2$) | 0.02 – 1.65 / 0.27 | 0.015 – 2.44 / 0.36 | 0.02 – 0.374 / 0.14 | 0.011 – 0.184 / 0.07 | 0.01 – 0.02 / 0.04 |
| Quartz content | 69.3 – 70.0 / 62.69 | 55.4 – 66.0 / 62.0 | 53.9 – 58.3 / 56.7 | 56.6 – 65.0 / 60.7 | 40.6 – 61.0 / 51.8 |
| Rock fragment contents | 8.2 – 19.4 / 11.6 | 5.7 – 19.7 / 10.5 | 11.2 – 16.7 / 15.3 | 9.2 – 16.3 / 13.4 | 15.0 – 17.6 / 16.6 |
| Matrix content | 2.1 – 9.44 / 5.06 | 1.7 – 7.56 / 4.73 | 4.6 – 10.2 / 6.5 | 3.7 – 9.6 / 6.9 | 5.0 – 11.5 / 7.8 |

PS: $\frac{MIN - MAX}{Average}$.

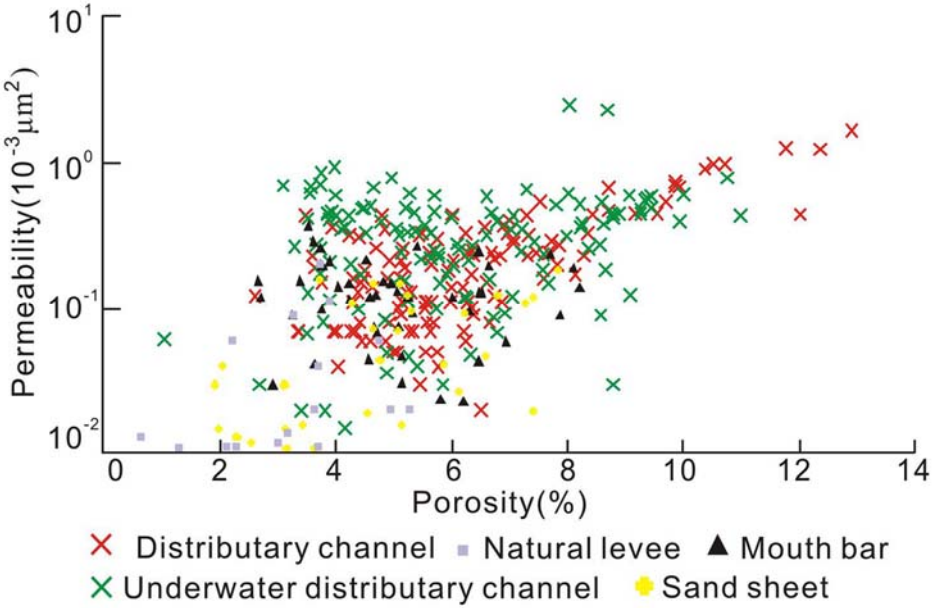


**Fig. 13**. Plot relationship of sandstone reservoir quality of different braided delta microfacies.

The sandstones of the distributary channel and underwater distributary channel of the Lower Shihezi Formation generally exhibit the coarsest grain sizes (pebbly coarse sandstones and medium sandstones). The content of quartz is very high. In contrast, the content of rock fragments and matrix is very low, and consequently, these two facies show the best physical reservoir properties.

The grain sizes of the mouth bar sediments are slightly smaller than those of the underwater distributary channels, and consist of medium to fine sandstones, with high contents in quartz and slightly higher matrix and rock fragment contents than in the underwater distributary channels. Therefore, the mouth bar deposits show medium physical reservoir properties.

The grain sizes of the sand sheets are relatively fine and the rocks are mainly siltstones. They contain high amounts of quartz, similar to the mouth bars, and show medium physical reservoir properties (slightly lower than those of the mouth bars).

The natural levees are dominated by siltstones with relatively low quartz contents but the highest matrix and rock fragment contents among the different microfacies types. In the analyzed samples, a high amount of the matrix and rock fragments is pressed into the primary pores by compaction. Therefore, the degree of pore reduction damage reaches up to 60–80% (Fig. 10A), making this microfacies the one with the lowest physical reservoir properties.

#### *5.3.4. Control of sedimentary microfacies on reservoir development*

Within the study area, the underwater distributary channel microfacies exhibits high original porosities, and high quartz contents and is conducive to anti-compaction. Therefore, after the early cementation and compaction during diagenesis, the primary pores remained well preserved and could effectively communicate pore fluid. Consequently, the pore fluid could stay in full contact with soluble minerals, resulting in a high number of dissolution pores. Therefore, residual intergranular pores, intergranular dissolved pores, and intragranular dissolved pores are the main pore types that can be observed in the underwater distributary channels, making this facies the one with the best reservoir properties (Fig. 14).

The grain sizes of mouth bars are slightly finer. On the other hand, the matrix and rock fragment contents are relatively high (in comparison to the underwater distributary channels). In general, the pore evolution model of this microfacies is similar to that of the underwater distributary channels, predominantly developing residual intergranular pores, intergranular dissolution pores, and intragranular dissolution pores. The reservoir quality of this microfacies is of medium quality (Fig. 14).

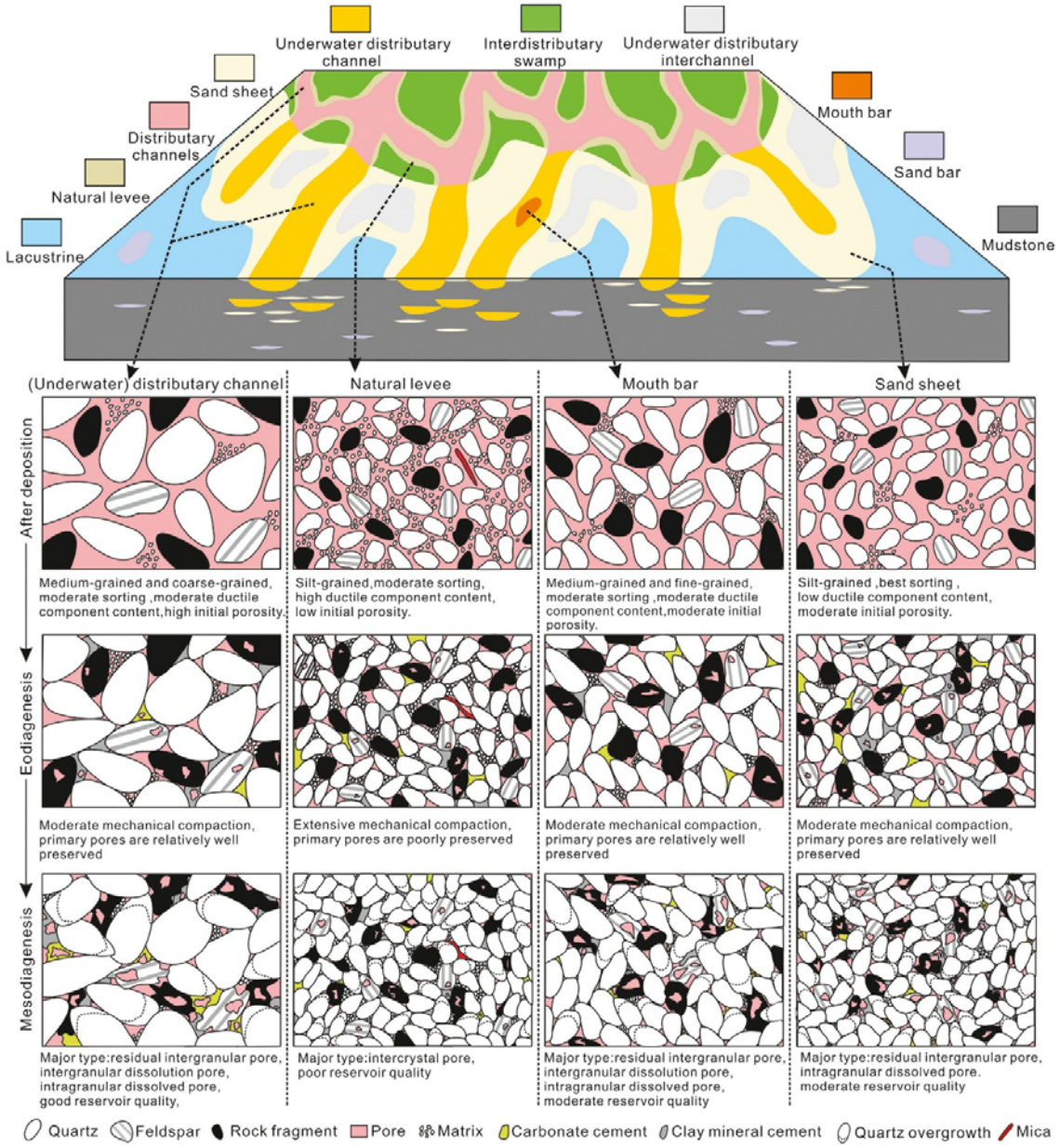


**Fig. 14.** Pore evolution model of sandstone reservoir in braided delta sedimentary system..

The quartz content of the sand sheet microfacies is high, but the grain size of its sandstones is relatively fine, and fine pore throats form relatively easily. However, the early compaction and cementation reduced the porosity, which was not beneficial for the entry of later fluids. The resulting pores are mainly residual intergranular pores and intragranular dissolved pores. This microfacies, therefore, exhibits medium reservoir quality (Fig. 14).

Finally, the reservoirs of the natural levee microfacies are made up of relatively fine grain sizes and exhibit high contents in matrix and rock fragments, and low original porosities. In addition, due to the early cementation and compaction, the original small primary pores are commonly filled with

cement and high amounts of matrix and rock fragments. These processes prevented the development of secondary pores. The main pore type that formed in this microfacies was intergranular pores. In consequence, this microfacies exhibits the lowest physical reservoir properties (Fig. 14).

In conclusion, it can be assumed that the environmental conditions existing during the time of deposition determine the physical and chemical characteristics of the clastic particles in a sandstone reservoir. Reservoirs that are formed by sandstones that developed in different or changing environments also exhibit heterogeneous characteristics, which have a significant impact on the resulting reservoir quality (Garzanti, 2019; Y. Li et al., 2021). Therefore, compared to the impact of the diagenetic processes, the depositional environment may be the main reason for the differences in reservoir quality, and the dominant factor controlling it.

## 6. Conclusions

The sandstone reservoir of the Lower Shihezi Formation is characterized by low porosities and low permeabilities. In general, the reservoir can be characterized as heterogeneous. To explore the causes of the above characteristics of the reservoir, this paper systematically studied the sedimentary facies and diagenesis. This not only provides an important basis for the exploration of the Lower Shihezi Formation but also sheds new light on the reasons for the reservoir heterogeneity. The conclusions are as follows:

1) Compaction and cementation during diagenesis reduced the physical properties of the reservoir with compaction causing the largest damage to the original pores. This may have been the main reason for the decrease in the physical properties and the formation of a tight sandstone reservoir.
2) Dissolution, however, led to the disintegration of feldspar, cuttings, and other particles and interstitial materials, resulting in the formation of secondary pores, which was conducive to an increase of the reservoir properties. Therefore, corresponding to increasing burial depths and influenced by different diagenetic processes, the physical properties of a reservoir can significantly change, leading to considerable reservoir heterogeneities.
3) Furthermore, differences in sedimentary facies are the dominant factor controlling sandstone reservoir quality. Differences in grain composition, grain size, and matrix content, typical for each microfacies and their distinctive pore evolution characteristics, resulted in unique physical reservoir properties for each microfacies. Consequently, the underwater distributary channel microfacies exhibits the best reservoir properties, followed by the mouth bar and sand sheet microfacies. The interdistributary swamp microfacies displays the lowest reservoir properties. The different microfacies play a significant role in controlling the reservoir quality and therefore form another major factor for reservoir heterogeneity.

## Declaration of competing interest

We declare that we have no financial and personal relationships with other people or organizations that can inappropriately influence our work, there is no professional or other personal interest of

any nature or kind in any product, service and/or company that could be construed as influencing the position presented in, or the review of, this manuscript.

## Acknowledgements

This study has been supported by the NSFC of China (Grant No. 41972146; 41402120). Editor Massimo Moretti and the reviewers are thanked for their constructive comments and very helpful reviews.

## References

Bjørlykke, K., 2014. Relationships between depositional environments, burial history and rock properties. Some principal aspects of diagenetic process in sedimentary basins. Sedimentary Geology 301, 1–14. https://doi.org/10.1016/j.sedgeo.2013.12.002.

Carroll, A.R., Grahamwand, S.A., Smith, M.E., 2010. Walled sedimentary basin of China. Basin Research 22, 17–22. https://doi.org/10.1111/j.1365-2117.2009.00458.x.

Cheng, L.X., Wang, L.J., Luo, Y.P., 2020. Research about distal-basin shallow-river fluvial-dominated delta mode of Xiaoheba formation of Silurian of Southeastern Sichuan Basin and thinking about oil and gas exploration. Petroleum 6 (3), 234–245. https://doi.org/10.1016/j.petlm.2020.05.001.

Crundwell, F.K., 2014. The mechanism of dissolution of minerals in acidic and alkaline solutions: part II. Application of a new theory to silicates, aluminosilicates and quartz. Hydrometallurgy 149, 265–275. https://doi.org/10.1016/j.

Curtis, M.E., Cardott, B.J., Songdergeld, C.H., Rai, C.S., 2012. Development of organic porosity in the Woodford Shale with increasing thermal maturity. International Journal of Coal Geology 103, 26–31. https://doi.org/10.1016/j.coal.2012.08.004.

Dutton, S.P., 2008. Calcite cement in Permian deep-water sandstones, Delaware Basin, west Texas: origin, distribution, and effect on reservoir properties. AAPG Bulletin 92, 765–787. https://doi.org/10.1306/01280807107.

Ehrenberg, S.N., 1989. Assessing the relative importance of compaction processes and cementation to reduction of porosity in sandstones: discussion; compaction and porosity evolution of Pliocene sandstones, Ventura Basin, California: discussion. AAPG Bulletin 73, 1274–1276. https://doi.org/10.1306/44b4aa1e-170a-11d7- 8645000102c1865d.

Folk, R.L., 1980. Petrology of Sedimentary Rocks. p. 182.

Fu, J.H., Wei, X.S., Nan, J.X., Shi, X.H., 2013. Characteristics and origin of reservoirs of gas fields in the Upper Paleozoic tight sandstone, Ordos Basin. Journal of Palaeogeography 15 (4), 529–538. https://doi.org/10.7605/gdlxb.2013.04.042 (In Chinese with English abstract).

Gaibor, J., Hochuli, J.P.A., Winkler, W., Toro, J., 2008. Hydrocarbon source potential of the Santiago Formation, Oriente Basin, SE of Ecuador. Journal of South American Earth Sciences 25 (2), 145–156. https://doi.org/10.1016/j.jsames.2007.07.002.

Garzanti, E., 2019. Petrographic classification of sand and sandstone. Earth Science Reviews 192, 545–563. https://doi.org/10.1016/j.earscirev.2018.12.014.

Ghanizadeh, A., Clarkson, C.R., Ardakani, S., Ardakani, O.H., Sanei, H., 2015. Petrophysical and geomechanical characteristics of Canadian tight oil and liquid-rich gas reservoirs: I. Pore network and permeability characterization. Fuel 153, 664–681. https://doi.org/10.1016/j.fuel.2015.03.020.

Hu, S.Y., Zhu, R.K., Wu, S.T., Bai, B., Yang, Z., Cui, J.W., 2018. Exploration and development of continental tight oil in China. Petroleum Exploration and Development 45 (4), 790–802. https://doi.org/10.1016/S1876-3804(18)30082-X.

Huang, S.J., Huang, K.K., Feng, W.L., Tong, H.P., Liu, L.H., Zhang, X.H., 2009. Mass exchanges among feldspar, kaolinite and illite and their influences on secondary porosity formation in clastic diagenesis — a case study on the upper paleozoic, Ordos basin and xujiahe formation, Western Sichuan depression. Geochimica 38, 498–506. https://doi.org/10.19700/j.0379-1726.2009.05.009 (in Chinese with English abstract).

Huang, Y.T., Kane, L.A., Zhao, Y., 2020. Effects of sedimentary processes and diagenesis on reservoir quality of submarine lobes of the Huangliu Formation in the Yinggehai Basin, China. Marine and Petroleum Geology 120, 104526. https://doi.org/10.1016/j.marpetgeo.2020.104526.

Jiang, Z.X., Liu, H., Zhang, S.W., Sun, X., Jiang, Z.L., 2010. Sedimentary characteristics of large-scale lacustrine beach-bars and their formation in the Eocene Boxing Sag of Bohai Bay Basin, East China. Sedimentology 58, 1087–1112. https://doi.org/10.1111/j.1365-3091.2010.01196.x.

Jiu, B., Huang, W.H., Li, Y., He, M.Q., 2021. Influence of clay minerals and cementation on pore throat of tight sandstone gas reservoir in the eastern Ordos Basin, China. Journal of Natural Gas Science and Engineering 87, 103762. https://doi.org/10.1016/j.jngse.2020.103762.

Li, Y., Hu, Z.W., 2014. Formation of the microcrystalline quartz coatings and its protection of the primary intergranular porosity in the deeply-buried sandstone reservoirs. Geological Science and Technology Information 33 (3), 87–92 (in Chinese with English abstract).

Li, Z., Hui, K., Li, L., 2008. Analysis of characteristics of gas migration and reservoir-forming in the upper paleozoic of northern Ordos basin. Journal of Mineralogy and Petrology 28, 77–83 (in Chinese with English abstract).

Li, Y.J., Zhao, Y., Yang, R.C., Fan, A.P., Li, F.P., 2010. Detailed sedimentary facies of a sandstone reservoir in the eastern zone of the Sulige gas field, Ordos Basin. Mining Science and Technology (China) 20 (6), 891–897. https://doi.org/10.1016/S1674-5264(09)60302-1.

Li, R., Zhang, D., Zhu, L.X., 2011. Densification of Upper Triassic Xujiahe tight sandstones, Western Sichuan, China. Petroleum Geology & Experiment 33 (03), 274–281 (in Chinese with English abstract).

Li, Y.L., Yu, X.H., Shan, X., Du, Y.H., Zhou, J.S., Han, X.Q., 2016. Provenance and sedimentary facies of He8 member of Xiashihezi formation in southeastern Ordos basin. Journal of Northeast Petroleum University 40 (03), 51–60 (in Chinese with English abstract).

Li, Y., Fan, A.P., Yang, R.C., Sun, Y.P., Nils, L., 2021a. Sedimentary facies control on sandstone reservoir properties: a case study from the permian Shanxi Formation in the southern Ordos basin, central China. Marine and Petroleum Geology 129, 105083. https://doi.org/10.1016/j.marpetgeo.2021.105083.

Li, S., Liu, L., Wu, J., Wang, L.L., Zhang, Z.L., 2021b. Diagenetic evolution of tight sandstone of Shanxi–Lower Shihezi formations in the southern Ordos Basin. Natural Gas Geoscience 32 (1), 47–56. https://doi.org/10.11764/j.issn.1672-1926.2020.09.008 (in Chinese with English abstract).

Li, J., Zhang, X., Tian, J.C., Liang, Q.S., Cao, T.S., 2021c. Effects of deposition and diagenesis on sandstone reservoir quality: a case study of Permian sandstones formed in a braided river sedimentary system, northern Ordos Basin, Northern China. Journal of Asian Earth Science 213 (15), 104745. https://doi.org/10.1016/j.jseaes.2021.104745.

Liang, F., Huang, W.H., Niu, J., 2018. Provenance analysis of Permain Shan1 and He 8 Formation in Permian in Southwest Ordos Basin. Acta Sedimentologica Sinica 36 (01), 142–153 (in Chinese with English abstract).

Liu, G.D., Sun, M.L., Zhao, Z.Y., Wang, X.B., Wu, S.H., 2013. Characteristics and accumulation mechanism of tight sandstone gas reservoirs in the Upper Paleozoic, northern Ordos Basin, China. Petroleum Science 10 (2013), 442–449. https://doi.org/10.1007/s12182-013-0294-1.

Liu, S.B., Huang, S.J., Shen, Z.M., Lv, Z.X., Song, R.C., 2014. Diagenetic fluid evolution and water-rock interaction model of carbonate cements in sandstone: an example from the reservoir sandstone of the Fourth Member of the Xujiahe Formation of the Xiaoquan–Fenggu area, Sichuan Province, China. Science China: Earth Sciences 57, 1077–1092. https://doi.org/10.1007/s11430-014-4851-2.

Ma, D.X., Xu, Y., Lv, J.W., Ji, H.J., Tuo, C.R., Hao, L.W., Su, L., Wang, Q., 2016. Relationship between provenance and formation of Lower Shihezi Formation in Linxing area, Ordos Basin, China. Natural Gas Geoscience 27 (7), 1215–1224 (in Chinese with English abstract).

Ma, B.Q., Chen, S.M., Yan, W.L., Li, C.Y., Zhang, H., Sun, Z.F., Zheng, J.D., Wang, Y., Wu, S.X., Wang, J.Y., 2021. Pore structure evaluation of low permeability clastic reservoirs based on sedimentation diagenesis: a case study of the Chang 8 reservoirs in the Zhenbei region, Ordos Basin. Journal of Petroleum Science and Engineering 196, 107841. https://doi.org/10.1016/j.petrol.2020.107841.

Madec, M., Espitalie, J., 1984. Application of pyrolysis to the characterization and the upgrading of the Toarcian oil shales from the Paris basin. Fuel 63, 1720–1725. https://doi.org/10.1016/0016-2361(84)90107-8.

Martini, I., Sandrelli, F., 2015. Facies analysis of a Pliocene river-dominated deltaic succession (Siena Basin, Italy): implications for the formation and infilling of terminal distributary channels. Sedimentology 62 (1), 234–265. https://doi.org/10.1111/sed.12147.

Masters, J.A., 1979. Deep Basin gas trap, western Canada. AAPG Bulletin 63 (2), 152–181. https://doi.org/10.1306/C1EA55CB-16C9-11D7-8645000102C1865D.

Morad, S., Al-Ramadan, K., Ketzer, J.M., De Ros, L.F., 2010. The impact of diagenesis on the heterogeneity of sandstone reservoirs: a review of the role of depositional facies and sequence stratigraphy. AAPG Bulletin 94, 1267–1309. https://doi.org/10.1306/04211009178.

Nazeer, A., Abbasi, S.A., Solangi, S.H., 2016. Sedimentary facies interpretation of Gamma Ray (GR) log as basic well logs in Central and Lower Indus Basin of Pakistan. Geodesy and Geodynamics 7 (6), 432–443. https://doi.org/10.1016/j.geog.2016.06.006.

Qian, W.D., Yin, T.J., Zhang, C.M., Hou, G.W., He, M., 2020. Diagenesis and diagenetic stages prediction of Ed2 reservoir in the west of Bozhong sag. Petroleum 6 (1), 23–30. https://doi.org/10.1016/j.petlm.2019.04.003.

Qin, Y., Yao, S.P., Xiao, H.M., Cao, J., Hu, W.X., Sun, L.H., Tao, K.Y., Liu, X.W., 2021. Pore structure and connectivity of tight sandstone reservoirs in petroleum basins: a review and application of new methodologies to the Late Triassic Ordos Basin, China. Marine and Petroleum Geology 129, 105084. https://doi.org/10.1016/j.marpetgeo.2021.105084.

Stonecipher, S., Winn, J., Bishop, M., 1984. Diagenesis of the Frontier Formation, Moxa Arch: a function of sandstone geometry, texture and composition, and fluid flux. AAPG Bulletin 68, 289–316. https://doi.org/10.1016/S0009-9120(02)00364-8.

Su, N.N., Song, F., Qiu, L.W., Zhang, W., 2021. Diagenetic evolution and densification mechanism of the Upper Paleozoic tight sandstones in the Ordos Basin, Northern China. Journal of Asian Earth Sciences 205, 104613. https://doi.org/10.1016/j.jseaes.2020.104613.

Sun, L.D., Zou, C.N., Jia, A.L., Wei, Y.S., Zhu, R.K., Wu, S.T., Guo, Z., 2019. Development characteristics and orientation of tight oil and gas in China. Petroleum Exploration and Development 46 (6), 1073–1087. https://doi.org/10.1016/S1876-3804(19)60264-8.

SY/T 5477, 2003. Petroleum and Gas Industry Standard, People's Republic of China. State of Economic and Trade commission (in Chinese).

Xiao, H.P., Liu, R.E., Zhang, F.D., Lin, C.S., Zhang, M.Y., 2019. Sedimentary model reconstruction and exploration significance of permian He 8 member in Ordos Basin, NW China. Petroleum Exploration and Development 46 (2), 280–292. https://doi.org/10.1016/S1876-3804(19)60008-X.

Xu, Q.H., Shi, W.Z., Xie, X.Y., Busbey, A.B., Xu, L., Wu, R., Liu, K., 2018. Inversion and propagation of the Late Paleozoic Porjianghaizi fault (North Ordos Basin, China): controls on sedimentation and gas accumulations. Marine and Petroleum Geology, 706–722 https://doi.org/10.1016/j.marpetgeo.2018.02.003.

Yang, H., Fu, J.H., Liu, X.S., Meng, P.L., 2012. Accumulation conditions and exploration and development of tight gas in the Upper Paleozoic of the Ordos Basin. Petroleum Exploration and Development 39 (3), 315–324. https://doi.org/10.1016/S1876-3804(12) 60047-0.

Yang, R.C., Van Loon, A.J., Jin, Z.J., Han, Z.Z., Fan, A.P., Liu, Q.Y., 2019. From divergent to convergent plates: resulting facies shifts along the southern and western margins of the sino-korean plate during the Ordovician. Journal of Geodynamics 129, 149–161. https://doi.org/10.1016/j.jog.2018.02.001.

Yang, S.F., Bao, Z.D., Wang, N., Qu, X.F., Lin, Y.B., Shen, J.J., Awan, R.S., 2020. Diagenetic evolution and its impact on reservoir quality of tight sandstones: a case study of the Triassic Chang 6 Member, Ordos Basin, northwest China. Marine and Petroleum Geology 117, 104360. https://doi.org/10.1016/j.marpetgeo.2020.104360.

Yu, X.H., Dorrik, S., Zeinab, S., Esentia, I., Brackenridge, R., Xie, X.N., Bankole, S., Ducassou, E., Llave, E., 2020. Contourite porosity, grain size and reservoir characteristics. Marine and Petroleum Geology 117, 104392. https://doi.org/10.1016/j. marpetgeo.2020.104392.

Zhang, W.Z., Guo, Y.R., Tang, D.Z., Zhang, J.F., Li, M., Xu, H., Lin, W.J., Tao, S., 2009. Characteristics of fluid inclusions and determination of gas accumulation period in the Upper Paleozoic reservoirs of Sulige Gas Field. Acta Petrolei Sinica 30 (5), 685–691. https://doi.org/10.7623/syxb200905009 (in Chinese with English abstract).

Zhang, H.B., Peng, J., Yang, S.J., Lu, M., Xia, Q.S., Li, B., 2016. Diagenesis and controlling factors of tight sandstone reservoirs: a case study of the lower member of Silurian Kepingtage Formation in Shuntuoguole area, Tarim Basin. Petroleum Geology & Experiment 38 (04), 543–550 (in Chinese with English abstract).

Zhang, Y.Y., Jiang, S., He, Z.L., Wang, Y.B., Guo, M.Q., Zhu, G.H., Cai, D.S., Lu, S.F., Xiao, D.S., Li, Y.C., Chen, G.H., 2021. Characteristics of heterogeneous diagenesis and modification to physical properties of Upper Paleozoic tight gas reservoir in eastern Ordos Basin. Journal of Petroleum Science and Engineering 208, 109243. https://doi.org/10.1016/j.petrol.2021.109243.

Zhao, J.Z., Fu, J.H., Yao, J.L., Liu, S.X., Wang, H.E., Cao, Q., Wang, X.M., Ma, Y.P., Fan, Y.F., 2012. Quasi-continuous accumulation model of large tight sandstone gas field in Ordos Basin. Acta Petrolei Sinica 33, 37–52 (in Chinese with English abstract).

Zou, C.N., Yang, Z., Tao, S.Z., Li, W., Wu, S.T., Hou, L.H., Zhu, R.K., Yuan, X.J., Wang, L., Gao, X.H., Jia, J.H., Guo, Q.L., 2012. Nano-hydrocarbon and the accumulation in coexisting source and reservoir. Petroleum Exploration and Development 39 (1), 15–32. https://doi.org/10.1016/S1876-3804(12)60011-1.

Zou, C.N., Yang, Z., He, D.B., Wei, Y.S., Li, J., Jia, A.L., Chen, J.J., Zhao, Q., Li, Y.L., Li, J., Yang, S., 2018. Theory, technology and prospects of conventional and unconventional natural gas. Petroleum Exploration and Development 45 (4), 604–618. https://doi.org/10.1016/S1876-3804(18)30066-1.